

Inverse Interscale Transport of the Reynolds Shear Stress in Plane Couette TurbulenceTakuya Kawata^{1,*} and P. Henrik Alfredsson^{2,†}¹*Tokyo University of Science, Yamazaki 2641, Noda, Chiba 278-8510, Japan*²*Linné Flow Centre, KTH Mechanics, Royal Institute of Technology, Stockholm SE-100 44, Sweden*

(Received 3 January 2018; published 12 June 2018)

Interscale interaction between small-scale structures near the wall and large-scale structures away from the wall plays an increasingly important role with increasing Reynolds number in wall-bounded turbulence. While the top-down influence from the large- to small-scale structures is well known, it has been unclear whether the small scales near the wall also affect the large scales away from the wall. In this Letter we show that the small-scale near-wall structures indeed play a role to maintain the large-scale structures away from the wall, by showing that the Reynolds shear stress is transferred from small to large scales throughout the channel. This is in contrast to the turbulent kinetic energy transport which is from large to small scales. Such an “inverse” interscale transport of the Reynolds shear stress eventually supports the turbulent energy production at large scales.

DOI: [10.1103/PhysRevLett.120.244501](https://doi.org/10.1103/PhysRevLett.120.244501)

In wall-bounded turbulence there exist large-scale vortical structures located away from the wall as well as small-scale structures in the wall vicinity. The large-scale structures are located in the logarithmic region or further out and have streamwise length scales far larger than those of the near-wall structures (see, for example, Ref. [1] and the reference therein). These large-scale structures are called “superstructures” or “very-large-scale motions,” and have been shown to account for a significant fraction of the total turbulent kinetic energy and the Reynolds shear stress [2,3].

The role of the large-scale structures becomes increasingly important with increasing Reynolds number in terms not only of their relative energy content but also of their interaction with the small-scale structures near the wall. Although the behavior of the near-wall structures has conventionally been considered universal when scaled by viscous units, the observed profiles of, for example, the turbulent intensities indicate a Reynolds number dependency [4–9]. The top-down influence from the large-scale structure further away from the wall has been intensively studied in the past decade and has been shown to affect the near-wall region [4,6,10–16], and thereby disproves strict viscous scaling there.

The other intriguing issue is whether the small-scale structures near the wall also affect the large-scale structures away from the wall. Iwamoto *et al.* [17] showed that the energy production by the mean velocity gradient is indispensable to maintain the large-scale structures, and other numerical experiments, such as Refs. [18–20], in which the smooth walls of turbulent channel flow were artificially replaced with other boundary conditions, demonstrated that the large-scale structures remain essentially unchanged irrespective of the flow structures near the wall. Consistently with this, Hwang and Cossu [21] showed

that the large-scale structures are self-sustainable even in the absence of the near-wall structures, and linear analysis also shows that amplified modes similar to the large-scale structures are found based on the mean flow profile (see, e.g., Refs. [22–24]). These earlier studies suggest that the large-scale structures essentially arise due to mean flow instabilities and are rather independent from the near-wall structures. On the other hand, Kim and Adrian [25] proposed that the large-scale structures are caused by successive mergers and/or growth of near-wall hairpin vortices. Toh and Itano [26] reported not only the top-down influence but also a bottom-up influence, i.e., from the near-wall to the large-scale structures, and concluded an interaction in “a cosupporting cycle.” However, the details of the interaction is still unclear.

From the viewpoint of the Reynolds-averaged turbulent statistics, the effect of such an interaction between the large- and small-scale structures may be expressed as an interscale and/or spatial transport of the Reynolds stresses at different scales. Such “scale-by-scale” analysis on the Reynolds stress transport is reported by, for example, Lee and Moser [16,27] and Mizuno [28], and the influence from the large-scale to near-wall structures is observed as a turbulent energy flux toward the wall. While only the turbulent kinetic energy transport is investigated in these studies, the Reynolds *shear* stress is also an essential quantity as it is the main (and in streamwise homogeneous flows the only) Reynolds stress component that appears in the streamwise mean momentum equation in wall turbulence. Thereby the transport of the Reynolds shear stress is an essential factor in understanding the structure of wall turbulence.

In this Letter we analyze the scale-by-scale transport of the Reynolds shear stress as well as the turbulent kinetic

energy, and show that the influence from the small scales near the wall indeed plays a role in maintaining the large-scale structures away from the wall. Our analysis is based on an experimental data set of plane Couette turbulence at some moderate Reynolds numbers from our previous work [29]. As observed in many earlier studies of turbulent plane Couette flow (see, e.g., Refs. [30–33]), large-scale vortical structures exist in the core region of the channel, and in the present study we focus on their interaction with small-scale structures.

We consider plane Couette flow where two parallel walls spatially separated by the distance $2h$ are translating in opposite directions with the same speed U_w . The origin of the coordinates is defined at the channel center and x , y , and z axes are taken in the streamwise, wall-normal, and spanwise directions. The Reynolds number is defined as $Re = U_w h / \nu$, where ν is the kinematic viscosity of the fluid. Three velocity components were measured by stereoscopic particle image velocimetry on the xz plane at $y/h = -0.83, -0.75, -0.67, -0.59, -0.46, -0.23, 0, 0.23, 0.46$. The measurements were done for $Re = 500, 1000, 1500, \text{ and } 2000$, which correspond to friction Reynolds numbers $Re_\tau = u_\tau h / \nu = 37, 63, 85, \text{ and } 108$, where u_τ is the friction velocity defined as $u_\tau = \sqrt{\tau_w / \rho}$ based on the wall shear stress τ_w and the fluid density ρ . The wall shear stress was evaluated from the sum of the mean shear and the Reynolds shear stress as detailed in Ref. [29]. About 300 statistically independent snapshots (separated by about 20 s, which is at least an order of magnitude larger than the integral timescale of the flow) of instantaneous velocity fields were obtained at each y position for evaluation of statistical quantities. Further details of the experiment are found in Refs. [29,34].

In order to investigate the interscale interaction, we make a large- or small-scale decomposition of the fluctuating velocity fields and derive the transport equation of each corresponding part of the Reynolds stress. The instantaneous velocities \tilde{u}_i are split into their mean values $U_i = \langle \tilde{u}_i \rangle$ and their deviations $u_i = \tilde{u}_i - U_i$. Here, $\langle \rangle$ indicates the averaged quantities in x and z directions and in time. The deviations u_i are further decomposed into a large- and a small-scale part by spatial filtering based on a spanwise cutoff wave number k_z as $u_i = u' + u''$, where superscripts $'$ and $''$ represent the large- and small-scale part, respectively. Since there is no overlapping wave number range between them, their cross-correlation is zero, $\langle u'_i u''_j \rangle = \langle u''_i u'_j \rangle = 0$, and the Reynolds stress is therefore simply decomposed into its large- and small-scale parts, $\langle u_i u_j \rangle = \langle u'_i u'_j \rangle + \langle u''_i u''_j \rangle$. In a similar manner as the transport equation of the “full” Reynolds stress $\langle u_i u_j \rangle$ is derived, one can derive those for $\langle u'_i u'_j \rangle$ and $\langle u''_i u''_j \rangle$ as

$$\frac{D\langle u'_i u'_j \rangle}{Dt} = P_{ij}^L - \varepsilon_{ij}^L + \Phi_{ij}^L + D_{ij}^{\nu,L} + D_{ij}^{t,L} - \text{Tr}_{ij}, \quad (1)$$

$$\frac{D\langle u''_i u''_j \rangle}{Dt} = P_{ij}^S - \varepsilon_{ij}^S + \Phi_{ij}^S + D_{ij}^{\nu,S} + D_{ij}^{t,S} + \text{Tr}_{ij}, \quad (2)$$

where P_{ij}^L , ε_{ij}^L , Φ_{ij}^L , and $D_{ij}^{\nu,L}$ on the right-hand side of Eq. (1) are the large-scale parts of production, viscous dissipation, velocity-pressure-gradient correlation, and viscous diffusion terms defined as

$$P_{ij}^L = -\langle u'_i u'_k \rangle \frac{\partial U_j}{\partial x_k} - \langle u'_j u'_k \rangle \frac{\partial U_i}{\partial x_k}, \quad \varepsilon_{ij}^L = 2\nu \left\langle \frac{\partial u'_i}{\partial x_k} \frac{\partial u'_j}{\partial x_k} \right\rangle,$$

$$\Phi_{ij}^L = -\frac{1}{\rho} \left(\left\langle u'_i \frac{\partial p'}{\partial x_j} \right\rangle + \left\langle u'_j \frac{\partial p'}{\partial x_i} \right\rangle \right), \quad D_{ij}^{\nu,L} = \nu \frac{\partial^2 \langle u'_i u'_j \rangle}{\partial x_k^2},$$

and their corresponding small-scale parts in Eq. (2) are those with the superscripts $'$ interchanged by $''$. The terms related with the interaction between the large- and small-scale part of the velocity field are the turbulent spatial transport terms,

$$D_{ij}^{t,L} = -\frac{\partial}{\partial x_k} (\langle u'_i u'_j u'_k \rangle + \langle u'_i u'_j u''_k \rangle + \langle u''_i u'_j u'_k \rangle + \langle u''_i u'_j u''_k \rangle), \quad (3)$$

$$D_{ij}^{t,S} = -\frac{\partial}{\partial x_k} (\langle u''_i u''_j u''_k \rangle + \langle u''_i u''_j u'_k \rangle + \langle u'_i u''_j u''_k \rangle + \langle u''_i u'_j u'_k \rangle), \quad (4)$$

and the interscale transport term,

$$\text{Tr}_{ij} = -\left\langle u''_i u''_k \frac{\partial u'_j}{\partial x_k} \right\rangle - \left\langle u'_j u''_k \frac{\partial u''_i}{\partial x_k} \right\rangle + \left\langle u'_i u'_k \frac{\partial u''_j}{\partial x_k} \right\rangle + \left\langle u'_j u'_k \frac{\partial u''_i}{\partial x_k} \right\rangle. \quad (5)$$

Here, $D_{ij}^{t,L}$ and $D_{ij}^{t,S}$ represent the spatial redistribution of $\langle u'_i u'_j \rangle$ and $\langle u''_i u''_j \rangle$, respectively, and Tr_{ij} indicates energy exchange between them. One can easily see that the sum of Eqs. (1) and (2) yields the transport equation of the full Reynolds stress $\langle u_i u_j \rangle$. An interesting feature of this formulation is that the first two terms and the others on the right-hand side of Eq. (5) have different signs and are similar to the production term, since they are products of the second moment of velocity fluctuations and velocity gradients. From the analogy to the Reynolds stress productions, one may interpret that the first two terms indicate the energy transfer from the larger to smaller scales, whereas the others represent the transfer in the other direction. It would also be worth mentioning here that the present formulation Eqs. (1)–(5) is valid not only for the large- or small-scale decomposition based on the Fourier modes, but also for any other decompositions that satisfy

$\langle u'_i u''_j \rangle = \langle u''_i u'_j \rangle = 0$, for example, those based on the proper orthogonal decomposition.

As the filtered Reynolds stresses $\langle u'_i u'_j \rangle$ are related to the Reynolds stress spectra as $E_{ij} = \partial \langle u'_i u'_j \rangle / \partial k_z$, differentiating Eq. (1) with respect to k_z yields the scale-by-scale transport equation of the Reynolds stress:

$$\frac{DE_{ij}}{Dt} = pr_{ij} - \epsilon_{ij} + \phi_{ij} + d_{ij}^v + d_{ij}^t + tr_{ij}, \quad (6)$$

where the terms on the right-hand side are the derivatives of the corresponding terms in Eq. (1). These terms except d_{ij}^t and tr_{ij} can be expressed by the Fourier velocity spectra or velocity-pressure-gradient cospectra and represent the spectral contribution from each scale to the overall production, dissipation, etc. The turbulent spatial transport $d_{ij}^t = \partial D_{ij}^t / \partial k_z$ and the interscale transport $tr_{ij} = -\partial \text{Tr}_{ij} / \partial k_z$ consist of different combinations of the triad interactions between the fluctuating velocities and velocity gradients, and are particularly focused on in the following analysis. d_{ij}^t represents spatial redistribution of the Reynolds stress at each scale: particularly in the present flow configuration, the integration of d_{ij}^t across the channel at a fixed scale k_z (or the corresponding λ_z) is zero for any scale. On the other hand, the interscale transport Tr_{ij} indicates, as seen from Eqs. (1) and (2), flux of the Reynolds stress from the large- to small-scale part of the flow field across wave number k_z in the Fourier space. Therefore, the derivative quantities $tr_{ij} = -\partial \text{Tr}_{ij} / \partial k_z$ represent the local gain or loss at k_z by such interscale transport.

Figure 1 presents the space-wavelength (y - λ_z) diagrams of the interscale transport of (a)–(c) the turbulent kinetic energy $\text{Tr}_{k_t} = \langle u_i u_i \rangle / 2$ and (d)–(f) the Reynolds shear stress $-\langle uv \rangle$ for different Reynolds numbers. For the wall-normal location

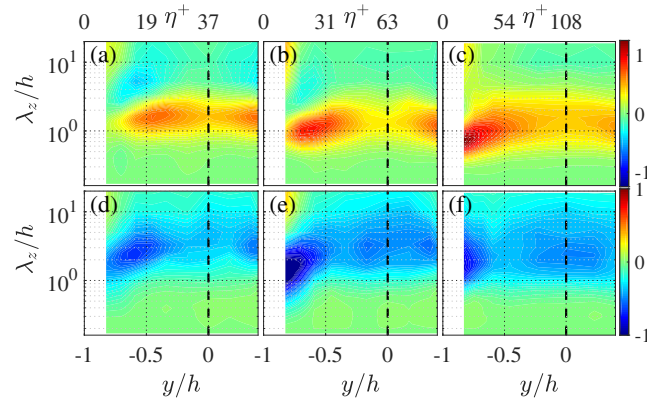


FIG. 1. Space-wavelength (y - or η - λ_z) diagrams of interscale transport of (a)–(c) the turbulent kinetic energy Tr_{k_t} and (d)–(f) the Reynolds shear stress Tr_{-uv} scaled by u_τ^3/h at (a), (d) $\text{Re} = 500$, (b), (e) 1000, and (c), (f) 2000. The black dashed line in each panel indicates the channel center $y/h = 0$.

of the data points the distance from the wall at $y/h = -1$ scaled by the wall units, $\eta^+ = yu_\tau/\nu + \text{Re}_\tau$, is also shown. It should be noted that for the turbulent kinetic energy transport Tr_{k_t} some terms on the right-hand side of Eq. (5) associated with $\partial/\partial y$ cannot be evaluated based on the present experimental data and therefore are omitted, while for the Reynolds shear stress transport Tr_{-uv} all terms can be evaluated since the wall-normal velocity gradients in Tr_{-uv} are all related with $\partial v'/\partial y$ or $\partial v''/\partial y$, which can be obtained via the continuity equation. As shown in Figs. 1(a)–1(c), Tr_{k_t} is generally positive, indicating that k_t is mainly transferred from larger to smaller scales as considered in the classical view of turbulent energy cascade. The positive peak is located at relatively small scales near the wall and its location is shown to move closer to the wall and also toward smaller scales (with respect to h) as Re increases.

Saikrishnan *et al.* [35] reported a net inverse energy cascade in the buffer layer by their analysis based on a two point scale energy budget. In the present study, however, we do not observe such inverse cascade in the corresponding region, but our results are instead in qualitative agreement with Ref. [28]. As we focus on the transport of the Reynolds shear stress, further investigation on the difference between such observations is beyond the scope of the present paper.

As presented in Figs. 1(d)–1(f), Tr_{-uv} shows negative values in the entire region of the channel, which indicates that $-\langle uv \rangle$ generally is transferred from smaller to larger scales in contrast to k_t . Such inverse interscale transport of $-\langle uv \rangle$ is significant in the near-wall region and increases in magnitude with the Reynolds number. Tr_{-uv} is also shown to have a negative peak at relatively large scales at the channel center for $\text{Re} \geq 1000$, and the location seems rather unchanged with increasing Re .

The scale-by-scale transport equation (6) is now investigated for k_t and $-\langle uv \rangle$. Figures 2(a1) and 2(b1) present the turbulent kinetic energy spectra E_{k_t} and the Reynolds shear stress cospectra E_{-uv} at the channel center for four different Reynolds numbers, respectively, and the scale-by-scale energy gain or loss by their production and interscale transport is given in Figs. 2(a2) and 2(b2). For all Reynolds numbers, both the energy spectra E_{k_t} and the cospectra E_{-uv} have their peaks around $\lambda_z/h = 3$, and the turbulent energy transport tr_{k_t} is shown to bring energy from the large-scale energy-containing range to smaller scales, while the shear stress transport tr_{-uv} indicates the opposite tendency. What should be noted here is that the Reynolds shear stress productions pr_{-uv} have their peaks at somewhat smaller scales compared to E_{-uv} itself, although the turbulent energy spectra E_{k_t} and its production pr_{k_t} have their peaks at the corresponding wavelengths. Such a tendency can also be seen in the results in Refs. [12,36] (see their Figs. 6 and 4, respectively, the wall-normal velocity spectra correspond to the shear-stress

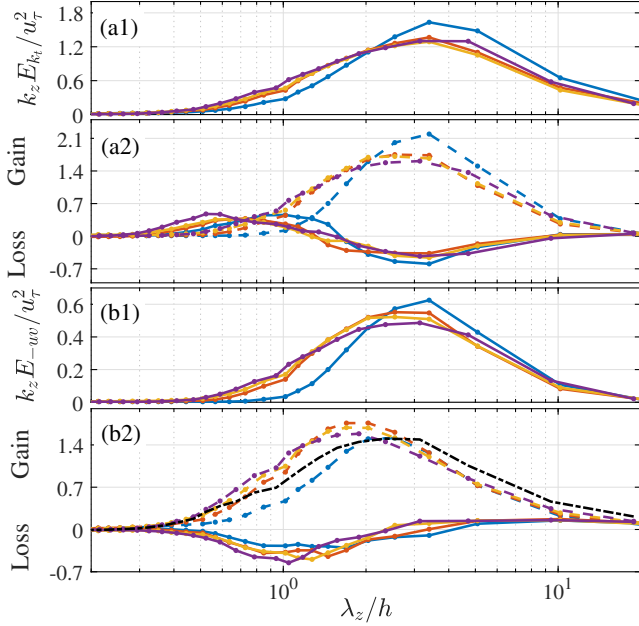


FIG. 2. Profiles at the channel center $y/h = 0$ of the premultiplied (a1) spectra of the turbulent kinetic energy $k_z E_{k_i}$, (b1) cospectra of the Reynolds shear stress $k_z E_{-uv}$, and (a2), (b2) their scale-by-scale production and interscale transport for four different Reynolds numbers. The values are scaled by u_τ^2 in (a1) and (b1) while scaled by u_τ^3/h in (a2) and (b2). The colors represent different Reynolds number cases: blue, $Re = 500$; red, $Re = 1000$; yellow, $Re = 1500$; purple, $Re = 2000$; and the dashed and solid lines in (a2) and (b2) present the premultiplied production and interscale transport, respectively. The black dash-dotted line in (b2) represents $k_z(pr_{-uv} + tr_{-uv} + d_{-uv}^l)$ for $Re = 2000$.

production spectra, as $pr_{-uv} = E_{vv}dU/dy$). The production of $-\langle uv \rangle$ occurs at relatively small scales because of the distribution of the wall-normal velocity spectra E_{vv} : unlike the streamwise Reynolds normal stress $\langle u^2 \rangle$, there is no production of the wall-normal component $\langle v^2 \rangle$, and it receives energy from $\langle u^2 \rangle$ via the pressure-strain redistribution at relatively small scales [27,28].

As clearly shown in Figs. 2(a2) and 2(b2), the turbulent energy spectra E_{k_i} and the Reynolds shear stress cospectra E_{-uv} at large scales are mainly generated through production by the mean flow, and the contributions by the interscale transport are small in comparison. This observation is consistent with earlier studies [17–24], which suggest that the large-scale structures away from the wall are essentially free from the influences by the near-wall structures and mainly generated by the mean flow instabilities. However, the peaks of E_{-uv} are shown to be located at somewhat larger scales than its production spectra. Such tendencies cannot only be explained by the local production by the mean velocity gradient, and thus imply an effect by the interscale transport that brings $-\langle uv \rangle$ from small to large scales.

Figure 3 presents the space-wavelength diagram of the Reynolds stress cospectra E_{-uv} along with its scale-by-scale production pr_{-uv} , interscale transport tr_{-uv} , and the turbulent spatial transport d_{-uv}^l for the highest Reynolds number case $Re = 2000$. As shown in Figs. 3(a) and 3(b), the shear stress cospectra E_{-uv} and the production spectra pr_{-uv} are significant in the corresponding wavelength range in the relatively near-wall region, while in the core region of the channel the E_{-uv} peaks are located at larger scales compared to those of the production pr_{-uv} . Figures 3(c) and 3(d) show that for all y positions the interscale transport tr_{-uv} removes $-\langle uv \rangle$ from the relatively small scales $\lambda_z/h \approx 0.9$ and brings it to large scales $\lambda_z/h \geq 3$, and at both these large and small scales the spatial transport d_{-uv}^l carries $-\langle uv \rangle$ from the near-wall region to the channel center. It is also seen that both tr_{-uv} and d_{-uv}^l have a negative peak at relatively small scales in the near-wall region, where a significant peak of the production pr_{-uv} is located. Comparing these distributions, one can interpret that $-\langle uv \rangle$ produced by pr_{-uv} at relatively small scales near the wall is transported to large scales at the channel center by the interscale and spatial transport tr_{-uv} and d_{-uv}^l . The sum of tr_{-uv} and d_{-uv}^l at the peak location of E_{-uv} at $y/h = 0$ is about 23% of the production pr_{-uv} .

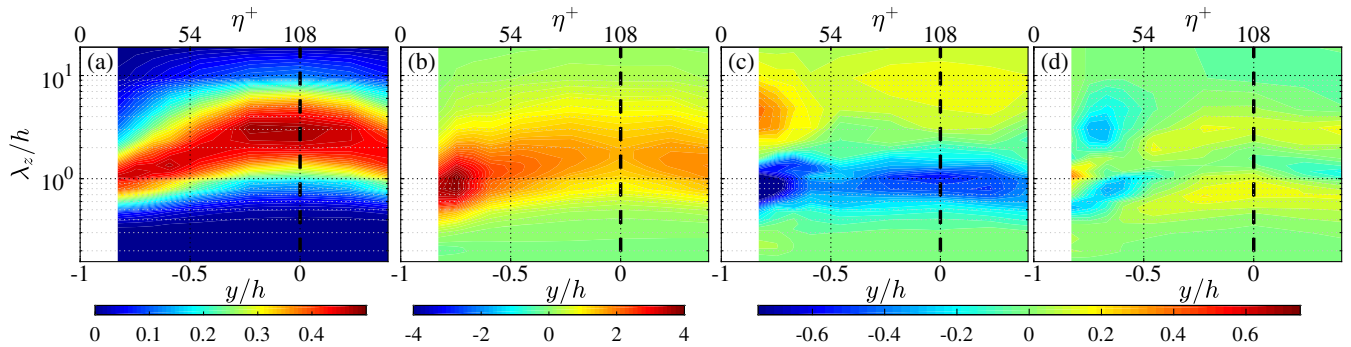


FIG. 3. Space-wavelength (y - or η - λ_z) diagrams of the premultiplied (a) Reynolds shear stress cospectra $k_z E_{-uv}$ and its scale-by-scale (b) production $k_z pr_{-uv}$, (c) interscale transport $k_z tr_{-uv}$, and (d) turbulent spatial transport $k_z d_{-uv}^l$ at $Re = 2000$. The values are scaled by u_τ^2 for $k_z E_{-uv}$ and by u_τ^3/h for the other quantities, and the black dashed line in each panel indicates the channel center $y/h = 0$.

The contribution by such $-\langle uv \rangle$ transport from the small scales near the wall to the large scales at the channel center is further depicted by the black dash-dotted line in Fig. 2(b2), which represents $pr_{-uv} + tr_{-uv} + d_{-uv}^t$ for $Re = 2000$. It is shown here that the peak location of pr_{-uv} alone is indeed shifted to the large-scale side by the addition of tr_{-uv} and d_{-uv}^t , and now the location corresponds well to the peak of E_{-uv} itself. Similar tendencies are also observed for the other Reynolds number cases, but not shown here for readability of the figure.

As described above, a certain influence from the small scales near the wall on the large-scale structure in the channel core region has been revealed in the present study through the analysis on the scale-by-scale transport of the Reynolds shear stress. Such interaction from small to large scales is not explicitly observed through the transport of the turbulent kinetic energy, but its productions at the large scales are partly supported by influences from the small scales through the Reynolds shear stress as $pr_{k_i} = E_{-uv} dU/dy$. The physical process of the Reynolds stress transport observed in the present study may correspond to the bottom-up influences from the near-wall to large-scale structures observed by Toh and Itano [26]. The present observations are limited to low Reynolds numbers (even at the highest Reynolds number case, $Re_\tau = 106$), and therefore call for further investigations on such interscale transport at higher Reynolds numbers.

This work was supported by Carl Tryggers Foundation for Scientific Research and KTH. T. K. also received Grant-in-Aid for Research Fellow No. 17J04115 by the Japan Society for the Promotion of Science (JSPS).

*kawata@rs.tus.ac.jp

†hal@mech.kth.se

- [1] A. J. Smits, B. J. McKeon, and I. Marusic, *Annu. Rev. Fluid Mech.* **43**, 353 (2011).
- [2] B. Ganapathisubramani, E. K. Longmire, and I. Marusic, *J. Fluid Mech.* **478**, 35 (2003).
- [3] J. H. Lee and H. J. Sung, *J. Fluid Mech.* **673**, 80 (2011).
- [4] S. Hoyas and J. Jimenez, *Phys. Fluids* **18**, 011702 (2006).
- [5] P. H. Alfredsson, R. Örlü, and A. Segalini, *Eur. J. Mech. B* **36**, 167 (2012).
- [6] S. Pirozzoli, M. Bernardini, and P. Orlandi, *J. Fluid Mech.* **680**, 534 (2011).
- [7] S. Pirozzoli, M. Bernardini, and P. Orlandi, *J. Fluid Mech.* **758**, 327 (2014).
- [8] P. Orlandi, M. Bernardini, and S. Pirozzoli, *J. Fluid Mech.* **770**, 424 (2015).
- [9] R. Örlü, T. Fiorini, A. Segalini, G. Bellani, A. Talamelli, and P. H. Alfredsson, *Phil. Trans. R. Soc. A* **375** (2017).
- [10] H. Abe, H. Kawamura, and H. Choi, *J. Fluids Eng.* **126**, 835 (2004).
- [11] N. Hutchins and I. Marusic, *Phil. Trans. R. Soc. A* **365**, 647 (2007).
- [12] J. Jiménez and S. Hoyas, *J. Fluid Mech.* **611**, 215 (2008).
- [13] R. Mathis, N. Hutchins, and I. Marusic, *J. Fluid Mech.* **628**, 311 (2009).
- [14] R. Mathis, J. P. Monty, N. Hutchins, and I. Marusic, *Phys. Fluids* **21**, 111703 (2009).
- [15] I. Marusic, R. Mathis, and N. Hutchins, *Int. J. Heat Fluid Flow* **31**, 418 (2010).
- [16] M. Lee and R. D. Moser, in *Proceedings of the 10th International Symposium on Turbulence and Shear Flow Phenomena, Chicago, 2017*, paper no. 9B-3, <http://www.tsfp-conference.org/proceedings/tsfp10-contents-of-volume-3.html>.
- [17] K. Iwamoto, N. Kasagi, and Y. Suzuki, in *Proceedings of the 6th WCCM in Conjunction with APCM'04* (Tsinghua University Press and Springer-Verlag, Beijing, China, 2004), paper no. MS022-174.
- [18] O. Flores and J. Jiménez, *J. Fluid Mech.* **566**, 357 (2006).
- [19] O. Flores, J. Jiménez, and J. C. del Álamo, *J. Fluid Mech.* **591**, 145 (2007).
- [20] Y. Mizuno and J. Jiménez, *J. Fluid Mech.* **723**, 429 (2013).
- [21] Y. Hwang and C. Cossu, *Phys. Rev. Lett.* **105**, 044505 (2010).
- [22] J. C. del Álamo and J. Jiménez, *J. Fluid Mech.* **559**, 205 (2006).
- [23] A. S. Sharma and B. J. McKeon, *J. Fluid Mech.* **728**, 196 (2013).
- [24] M. de Giovanetti, H. J. Sung, and Y. Hwang, *J. Fluid Mech.* **832**, 483 (2017).
- [25] K. C. Kim and R. J. Adrian, *Phys. Fluids* **11**, 417 (1999).
- [26] S. Toh and T. Itano, *J. Fluid Mech.* **524**, 249 (2005).
- [27] M. Lee and R. D. Moser, in *Proceedings of the 9th International Symposium on Turbulence and Shear Flow Phenomena, Melbourne, 2015*, paper no. 4A-3, <http://www.tsfp-conference.org/proceedings/tsfp9-contents-of-volume-2.html>.
- [28] Y. Mizuno, *J. Fluid Mech.* **805**, 171 (2016).
- [29] T. Kawata and P. H. Alfredsson, *Phys. Fluids* **1**, 034402 (2016).
- [30] M. J. Lee and J. Kim, in *Proceedings of the 8th International Symposium on Turbulent Shear Flows, Munich, 1991*.
- [31] J. Komminaho, A. Lundbladh, and A. V. Johansson, *J. Fluid Mech.* **320**, 259 (1996).
- [32] O. Kitoh, K. Nakabayashi, and F. Nishimura, *J. Fluid Mech.* **539**, 199 (2005).
- [33] T. Tsukahara, H. Kawamura, and K. Shingai, *J. Turbul.* **7**, N19 (2006).
- [34] T. Kawata and P. H. Alfredsson, *J. Fluid Mech.* **791**, 191 (2016).
- [35] N. Saikrishnan, E. D. Angelis, E. K. Longmire, I. Marusic, C. M. Casciola, and R. Piva, *Phys. Fluids* **24**, 015101 (2012).
- [36] R. Baidya, J. Philip, N. Hutchins, J. P. Monty, and I. Marusic, *Phys. Fluids* **29**, 020712 (2017).